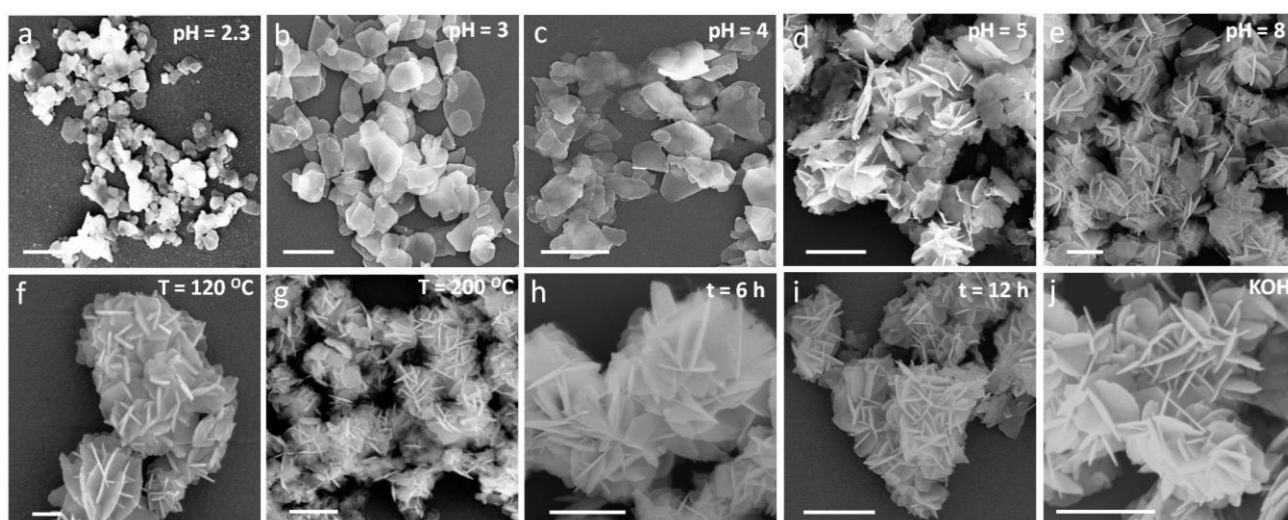


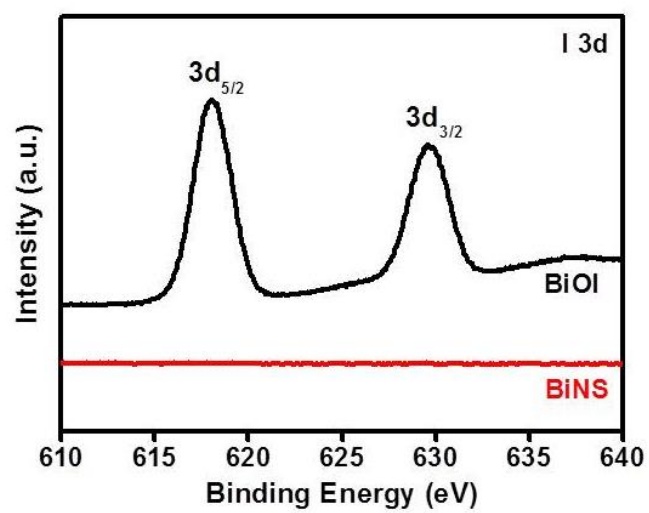
# **Supplementary Information**

Ultrathin Bismuth Nanosheets from In-Situ Topotactic Transformation for Selective Electrocatalytic  
Carbon Dioxide Reduction to Formate

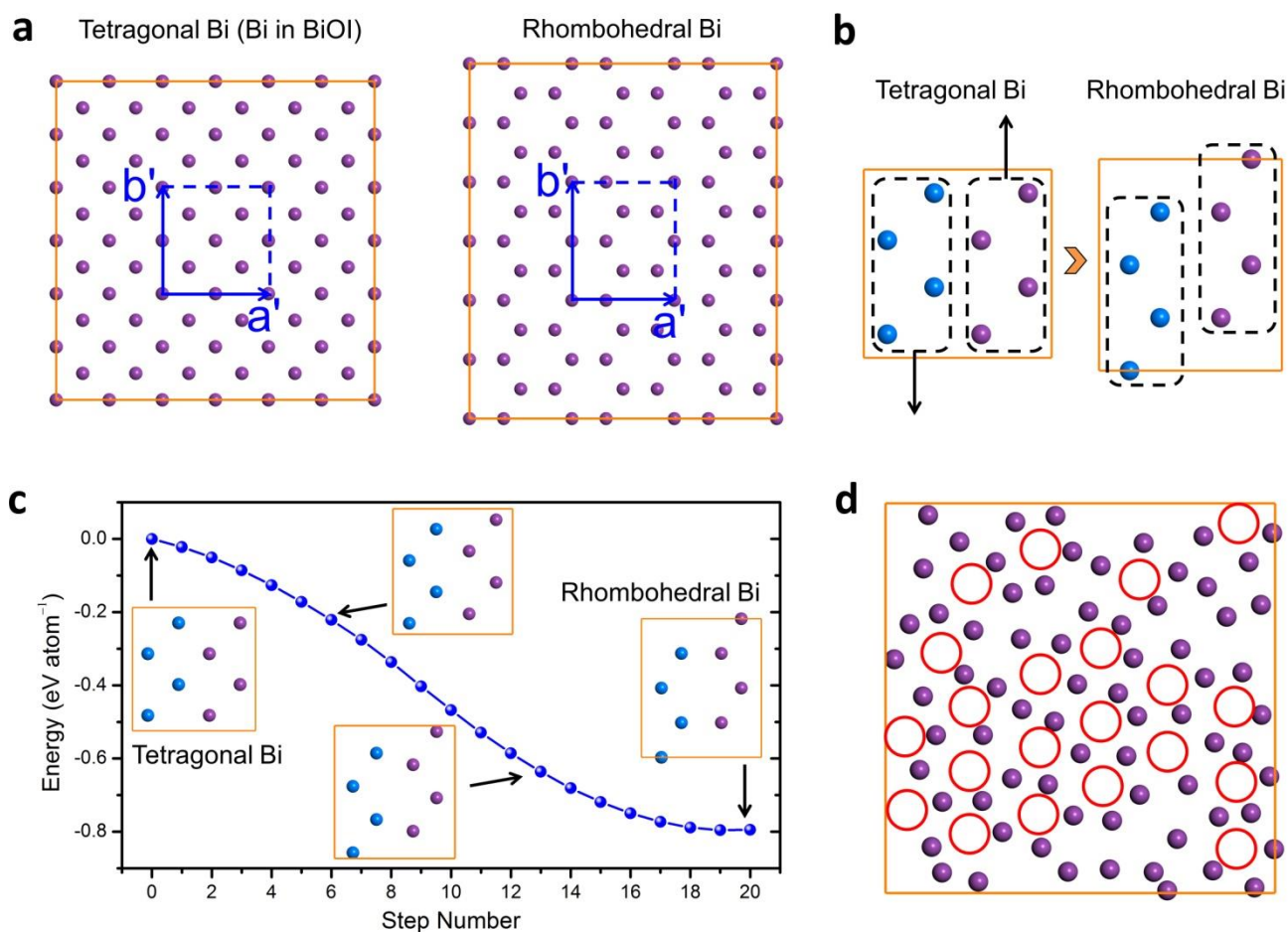
By Han et al.



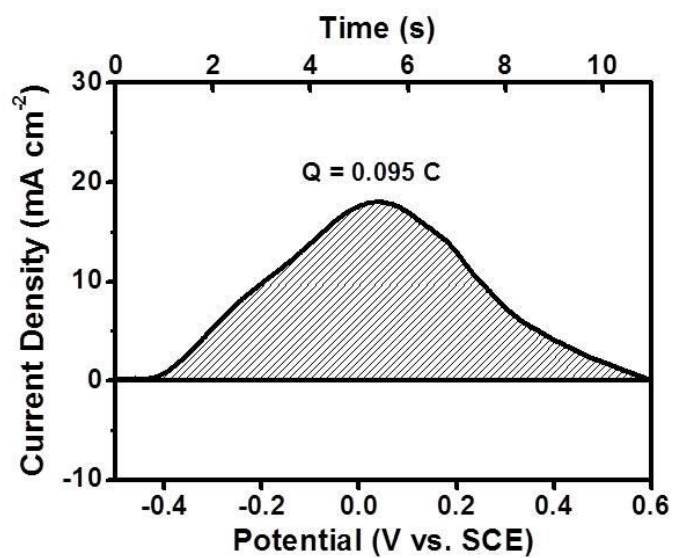
**Supplementary Figure 1. SEM images of BOI products from different synthetic conditions. (a-e)** different pHs, **(f,g)** different reaction temperatures, **(h,i)** different reaction times, and **(j)** KOH instead of NaOH, all under otherwise identical conditions as described in our Experimental Methods. Scale bar, 2  $\mu\text{m}$  (**a-e**); 200 nm (**f**); 1  $\mu\text{m}$  (**g-j**).



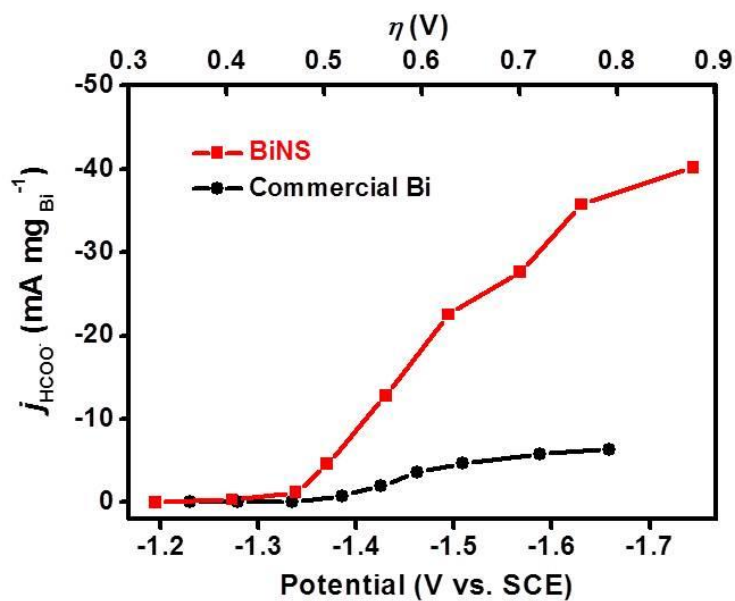
**Supplementary Figure 2. I 3d XPS spectra of BiOI and BiNS.**



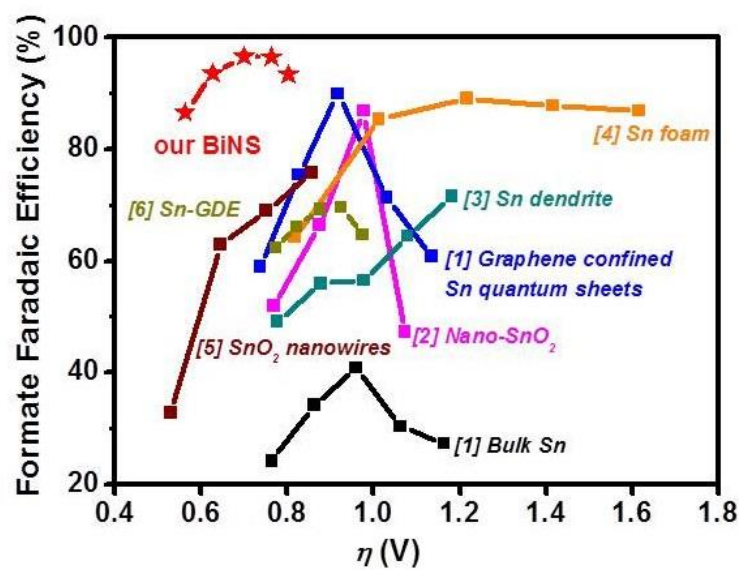
**Supplementary Figure 3. Theoretical insights on the topotactic conversion from BiOI to Bi.** (a) Arrangement of Bi atoms within the (001) plane of (left) tetragonal BiOI and (right) rhombohedral Bi;  $a'$  and  $b'$  represent the lattice vectors of supercells. (b) Schematic illustration showing the transformation from tetragonal Bi to rhombohedral Bi by sliding Bi atoms along the  $b'$ -direction. (c) Energy change during the transformation from tetragonal Bi to rhombohedral Bi, suggesting that once reduced, the conversion from BiOI to Bi is spontaneous. (d) Structural snapshot of original tetragonal Bi nanosheet after 1000 steps (1ps) of first-principles molecular dynamics simulation; red rings represent hexatomic Bi rings formed.



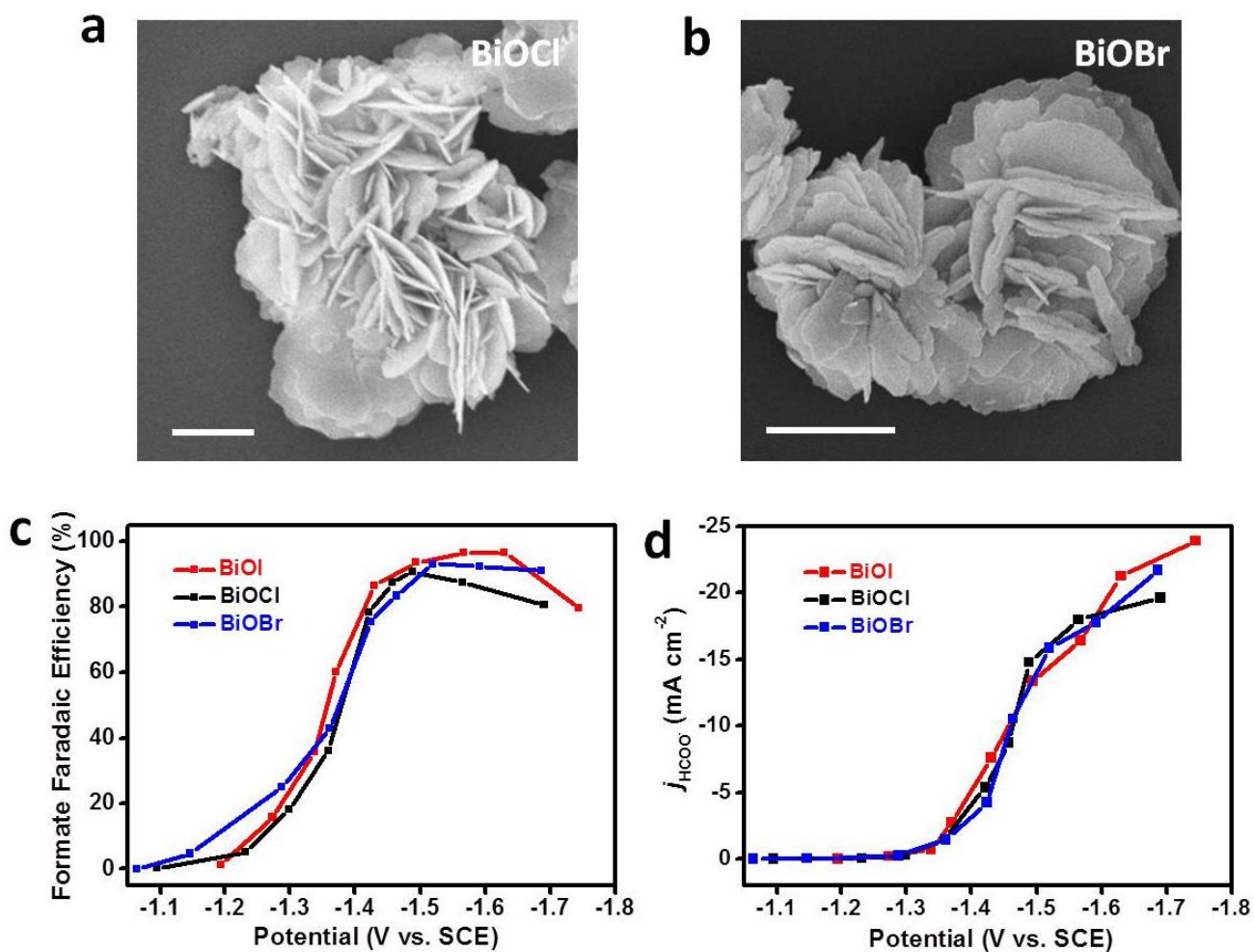
**Supplementary Figure 4.** Total charge integrated from the  $\text{Bi}^{3+}/\text{Bi}^0$  cathodic wave. Using this value, we further estimated the percentage of surface Bi sites.



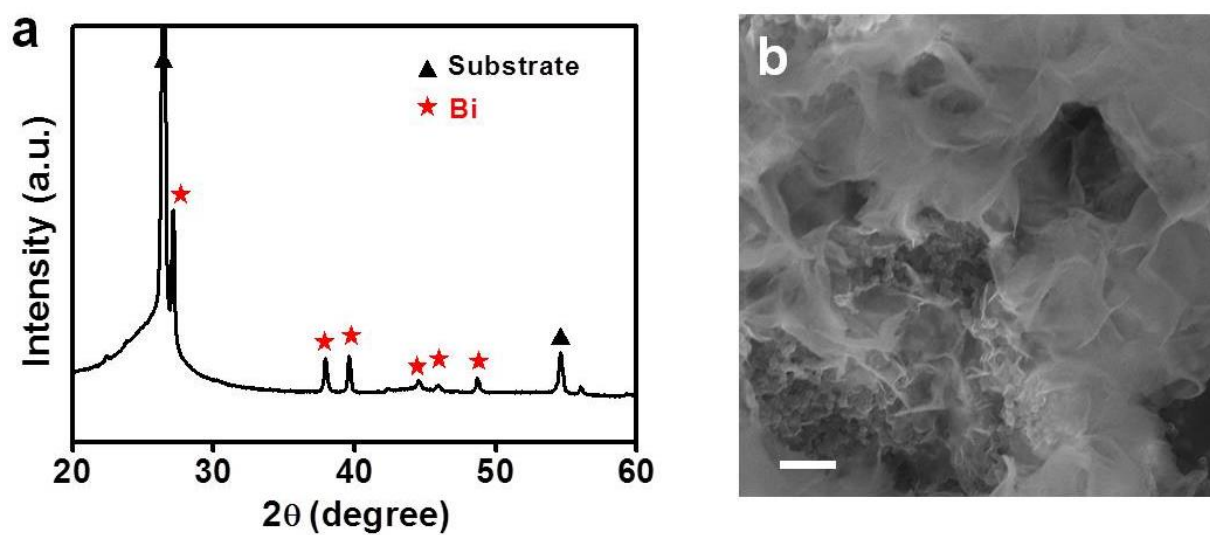
**Supplementary Figure 5. Mass-specific formate partial current density of BiNS and commercial Bi nanopowder.**



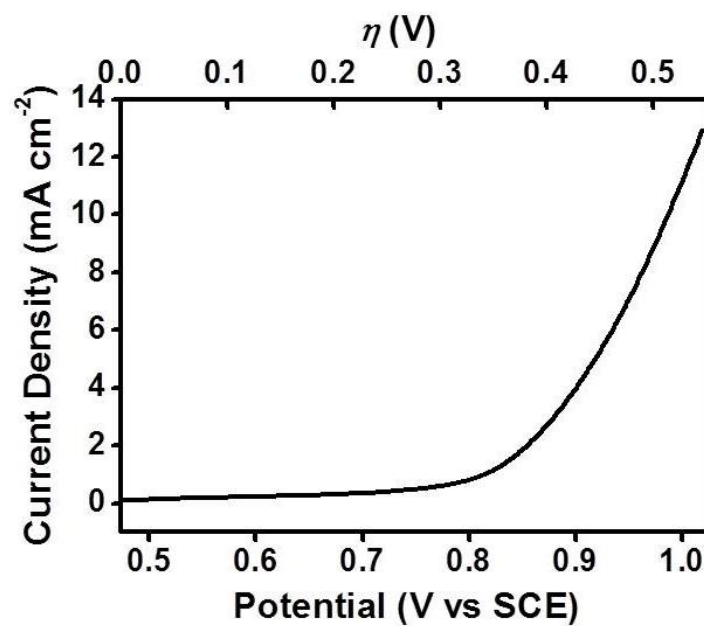
Supplementary Figure 6. Comparison on the formate Faradaic efficiency of BiNS and Sn-based CO<sub>2</sub>RR electrocatalysts. Refer to the Supplementary References at the end for more information.



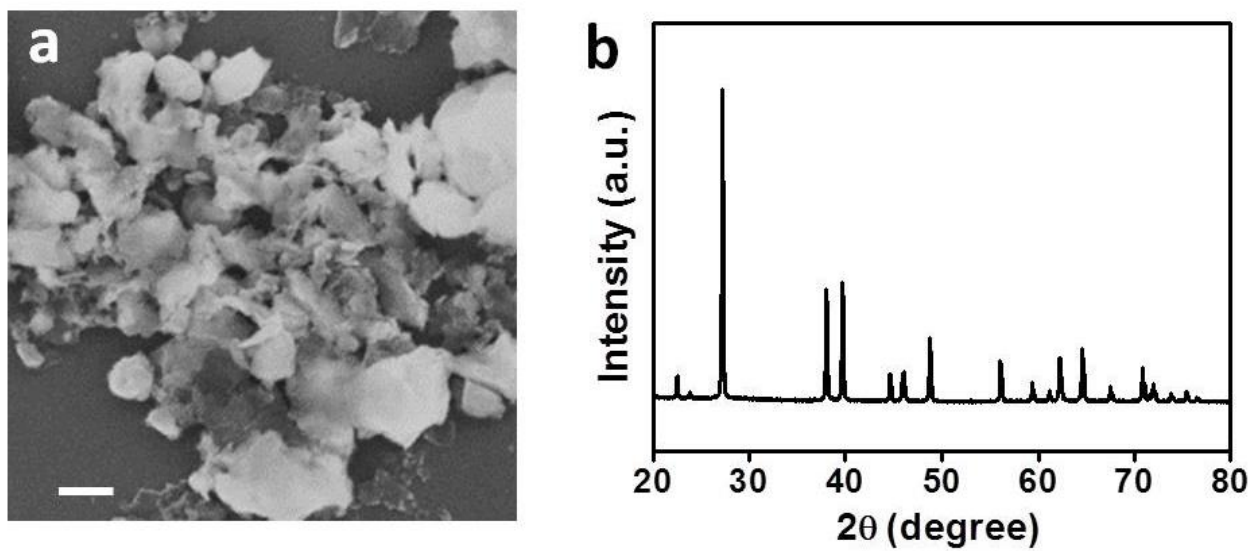
**Supplementary Figure 7. The effect of different halides.** (a,b) SEM images of BiOCl and BiOBr nanostructures using KCl or KBr as the halide precursor instead of KI under otherwise identical conditions as described in our Experimental Methods. (c) Formate Faradaic efficiency and (d) partial current density of Bi nanosheets derived from BiOCl and BiOBr in comparison with BiNS derived from BiOI. Scale bar, 1  $\mu\text{m}$  (a,b).



**Supplementary Figure 8. Postmortem characterizations of BiNS after the amperometric stability test. (a) XRD pattern; (b) SEM image. Scale bar, 500 nm (b).**



**Supplementary Figure 9. Polarization curve of Ir/C for OER electrocatalysis in 0.5 M NaHCO<sub>3</sub>.**



**Supplementary Figure 10. Structural characterizations of commercial Bi nanopowder. (a)** SEM image; **(b)** XRD pattern. Scale bar, 200 nm **(a)**.

**Supplementary Table 1.** Zero-point energy correction ( $E_{\text{ZPE}}$ ), entropy contribution ( $TS$ ), and the total free energy correction ( $G-E_{\text{elec}}$ ) for the studied system.

Species	$E_{\text{ZPE}}$ (eV)	$-TS$ (eV)	$G-E_{\text{elec}}$ (eV)
<b>H<sub>2</sub></b>	0.27	−0.40	−0.13
<b>H<sub>2</sub>O</b>	0.56	−0.67	−0.11
<b>CO<sub>2</sub></b>	0.31	−0.66	−0.35
<b>HCOOH</b>	0.89	−0.89	0.00
<b>CO</b>	0.13	−0.61	−0.48
<b>H*</b>	0.14	−0.03	0.11
<b>COOH*</b>	0.59	−0.29	0.30
<b>OCHO*</b>	0.58	−0.33	0.25

**Supplementary Table 2.** Analysis of reaction enthalpies (in eV) of gas-phase thermochemical reactions.  $\Delta H_{\text{ref}}$  was the literature values taken from NIST,  $\Delta H_{\text{cal}}$  was PBE calculated reaction enthalpies,  $\Delta H_{\text{cor}}$  was corrected reaction enthalpies that included  $-0.24$  eV for CO and  $+0.17$  eV for  $\text{CO}_2$  and  $\text{HCOO}^-$ , and error was defined as the energy difference between  $\Delta H_{\text{cor}}$  and  $\Delta H_{\text{ref}}$ .

Stoichiometry	$\Delta H_{\text{ref}}$	$\Delta H_{\text{cal}}$	$\Delta H_{\text{ref}} - \Delta H_{\text{cal}}$	$\Delta H_{\text{cor}}$	Error
$\text{CO}_2 + \text{H}_2 \rightarrow \text{CO} + \text{H}_2\text{O}$	0.43	0.84	0.41	0.43	0.00
$\text{CO}_2 + 4\text{H}_2 \rightarrow \text{CH}_4 + 2\text{H}_2\text{O}$	-1.71	-1.48	0.17	-1.71	0.00
$\text{CO} + 3\text{H}_2 \rightarrow \text{CH}_4 + \text{H}_2\text{O}$	-2.14	-2.35	-0.24	-2.14	0.00
$\text{CO}_2 + \text{H}_2 \rightarrow \text{HCOOH}$	0.15	0.15	0.00	0.15	0.00
$\text{CO} + \text{H}_2\text{O} \rightarrow \text{HCOOH}$	-0.27	-0.68	-0.41	-0.27	0.00
$\text{CO}_2 + 3\text{H}_2 \rightarrow \text{CH}_3\text{OH} + \text{H}_2\text{O}$	-0.55	-0.39	0.16	-0.56	0.01
$\text{CO} + 2\text{H}_2 \rightarrow \text{CH}_3\text{OH}$	-0.98	-1.23	-0.25	-0.99	0.01
$\text{CO}_2 + 3\text{H}_2 \rightarrow 1/2\text{C}_2\text{H}_4 + 2\text{H}_2\text{O}$	-0.66	-0.43	0.17	-0.66	0.00
$\text{CO} + 2\text{H}_2 \rightarrow 1/2\text{C}_2\text{H}_4 + \text{H}_2\text{O}$	-1.09	-1.30	-0.24	-1.09	0.00
$\text{CO}_2 + 7/2\text{H}_2 \rightarrow 1/2\text{C}_2\text{H}_6 + 2\text{H}_2\text{O}$	-1.37	-1.14	0.17	-1.37	0.00
$\text{CO} + 5/2\text{H}_2 \rightarrow 1/2\text{C}_2\text{H}_6 + \text{H}_2\text{O}$	-1.80	-2.01	-0.24	-1.80	0.00

## Supplementary References

1. Lei F., *et al.* Metallic tin quantum sheets confined in graphene toward high-efficiency carbon dioxide electroreduction. *Nat. Commun.* **7**, 12697 (2016).
2. Zhang S., Kang P., Meyer T. J. Nanostructured tin catalysts for selective electrochemical reduction of carbon dioxide to formate. *J. Am. Chem. Soc.* **136**, 1734-1737 (2014).
3. Won D. H., Choi C. H., Chung J., Chung M. W., Kim E. H., Woo S. I. Rational design of a hierarchical tin dendrite electrode for efficient electrochemical reduction of CO<sub>2</sub>. *ChemSusChem* **8**, 3092-3098 (2015).
4. Du D., *et al.* Achieving both high selectivity and current density for CO<sub>2</sub> reduction to formate on nanoporous tin foam electrocatalysts. *ChemistrySelect* **1**, 1711-1715 (2016).
5. Kumar B., *et al.* Reduced SnO<sub>2</sub> porous nanowires with a high density of grain boundaries as catalysts for efficient electrochemical CO<sub>2</sub>-into-HCOOH conversion. *Angew. Chem. Int. Ed.* **56**, 3645-3649 (2017).
6. Irtem E., *et al.* Low-energy formate production from CO<sub>2</sub> electroreduction using electrodeposited tin on GDE. *J. Mater. Chem. A.* **4**, 13582-13588 (2016).